J. Fluid Mech. (1990), *vol.* 215, *pp.* 289–307
Printed in Great Britain

On three-dimensional long water waves in a channel with sloping sidewalls

By J. MATHEW AND T. R. AKYLAS
Department of Mechanical Engineering, Massachusetts Institute of Technology, Cambridge, MA 02139, USA

(Received 11 August 1989)

A theoretical model is presented for the propagation of long, weakly nonlinear water waves along a channel bounded by sloping sidewalls, on the assumption that $h_0/w \ll 1$, where $2w$ is the channel width and h_0 is the uniform water depth away from the sidewalls. Owing to the non-rectangular channel cross-section, waves are three-dimensional in general, and the Kadomtsev–Petviashvili (KP) equation applies. When the sidewall slope is $O(1)$, an asymptotic wall boundary condition is derived, which involves a single parameter, $\mathscr{A} = A/h_0^2$, where A is the area under the depth profile. This model is used to discuss the development of an undular bore in a channel with trapezoidal cross-section. The theoretical predictions are in quantitative agreement with experiments and confirm the presence of significant three-dimensional effects, not accounted for by previous theories. Furthermore, the response due to transcritical forcing is investigated for $0 < \mathscr{A} \leqslant 1$; the nature of the generated three-dimensional upstream disturbance depends on $\mathscr{A}$ crucially, and is related to the three-dimensional structure of periodic nonlinear waves of permanent form. Finally, in an Appendix, the appropriate asymptotic wall boundary condition is derived for the case when the sidewall slope is $O(h_0/w)^{\frac{1}{3}}$.

1. Introduction

Long-crested, weakly nonlinear water waves can be modelled by the Korteweg–de Vries (KdV) equation in various contexts. The simplest case is that of entirely straight-crested waves propagating along a channel of uniform rectangular cross-section (see, for example, Whitham 1974, §13.11). On the further assumption that the channel width is comparable with the water depth, the KdV equation also describes long waves in a uniform channel of arbitrary cross-section (Peregrine 1968; Fenton 1973). In this instance, the wave disturbance is quasi-two-dimensional; a relatively small spanwise variation in the wave elevation is present, but the wave crests remain straight, and the KdV equation is still valid to leading order. Experimental confirmation of the theory was provided by Peregrine (1969) for solitary waves in channels with trapezoidal cross-section.

Peregrine (1968) noted, however, that the KdV theory breaks down when the channel width is much larger than the water depth; as the channel width is increased, spanwise variations become relatively large, giving rise to non-uniformities in the perturbation expansion. This is consistent with the earlier experimental observations of Sandover & Taylor (1962), who studied the development of undular bores in trapezoidal channels of moderately large width – about six to seven times the water depth. They pointed attention to the three-dimensional structure of wave disturbances; in particular, the presence of wave-crest curvature across the channel

and the tendency for waves to have irregular forms (except at very low discharge) cannot be explained by the KdV theory (Fenton 1973).

In this paper, a theoretical model is presented for long waves propagating along a channel of uniform non-rectangular cross-section, allowing for the presence of significant three-dimensional effects. The channel is assumed to be wide, $h_0/w \ll 1$, where $2w$ is the channel width at the undisturbed free surface and h_0 is the constant water depth away from the sidewalls. The approximate governing equations and boundary conditions are derived from the full water-wave theory, using matched asymptotic expansions†: the main body of fluid, away from the sloping boundaries, forms an 'outer' region where waves satisfy the Kadomtsev–Petviashvili (KP) equation, so that three-dimensional effects balance with nonlinear and dispersive effects; close to each sidewall, where the depth varies, there is an 'inner' region. Matching between the corresponding inner and outer expansions gives the appropriate asymptotic boundary condition for the KP equation at each sidewall, depending on the relative size of the inner region: when the wall slope is $O(1)$, as in the experiments of Sandover & Taylor (1962), this boundary condition involves only a single parameter, $\mathscr{A} = A/h_0^2$, A being the area under the depth profile; for wall slopes $O(h_0/w)^{\frac{1}{2}}$, the inner region is relatively thicker, and the appropriate boundary condition obtains a different form which depends more seriously on the details of the depth profile, as discussed in the Appendix. Finally, when the wall slope is very gentle, $O(h_0/w)$, there is no distinction between an inner and outer region any more, and one can use a KP equation with variable coefficients to account for depth variations; this possiblility has been discussed in a number of recent studies (see, for example, Kirby, Philip & Vengayil 1987; David, Levi & Winternitz 1989) and will not be considered here.

The present theory is used to discuss the development of an undular bore in a channel with trapezoidal cross-section, modelling the experimental set-up of Sandover & Taylor (1962). The theoretical predictions confirm the presence of significant three-dimensional effects, and are in quantitative agreement with experiment until wave breaking, which is not taken into account in the theory, occurs. In addition, the response to a slender pressure distribution, moving with transcritical speed at the free surface along the channel centreline is investigated. In a channel with vertical sidewalls, the corresponding problem has been studied in detail, both theoretically and experimentally, in recent years (see, for example, Wu 1987; Akylas 1988), and it is now known that periodic generation of straight-crested solitons takes place upstream. It is of interest, then, to see how sloping sidewalls affect this upstream response. Not surprisingly, the upstream disturbance is found to be three-dimensional in general; however, quite remarkably, as the parameter $\mathscr{A}$ is increased ($0 \leqslant \mathscr{A} \leqslant 1$), the regular, periodic form of the upstream response found in a channel with vertical sidewalls ($\mathscr{A} = 0$) disappears, and then reappears, while the individual waves acquire a far more complicated, three-dimensional structure. This loss and reappearance of uniformity in the upstream response seems to be related to the three-dimensional structure of periodic nonlinear waves of permanent form.

† Matching between an 'edge layer' close to a beach and an 'outer' shallow sea was previously used by Sugimoto & Kakutani (1984) to describe the normal incidence of a soliton.

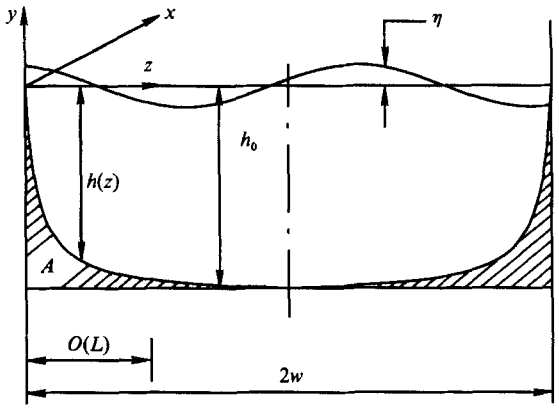

FIGURE 1. Channel cross-section.

2. Formulation

Consider an infinitely long channel of uniform cross-section. Cartesian coordinates are chosen such that y is directed vertically upward, x is along, and z is across the channel. The undisturbed free surface is at $y = 0, 0 < z < 2w$, where $2w$ is the channel width. The rigid bottom is at $y = -h(z)$; moreover, the cross-section is assumed to be such that the undisturbed water depth is a constant h_0 everywhere, except in the vicinity of the sidewalls where it decreases from h_0 to zero over a distance $O(L)$ with $L \ll w$ (see figure 1).

In setting up our asymptotic theory, it proves most economical to consider the generation of long waves by a pressure distribution moving with transcritical speed along the channel at the free surface; the propagation of free waves can be formulated as a special case. In the frame of reference following the applied pressure p, a uniform current of speed U exists in the water. Assuming inviscid, irrotational flow, gravity waves are described in terms of the free-surface elevation $y = \eta(x, z, t)$ and the velocity potential $\Phi = Ux - \frac{1}{2}U^2t + \phi(x, y, z, t)$; as usual, the perturbation potential ϕ satisfies Laplace's equation in the fluid and the familiar kinematic and dynamic boundary conditions hold at the free surface. Dimensionless (primed) variables are introduced as follows:

$$x = lx', \quad y = h_0 y', \quad z = h_0 z', \quad t = \left(\frac{l}{c_0}\right)t', \quad \eta = a\eta', \quad h = h_0 h',$$

$$\phi = \left(\frac{alc_0}{h_0}\right)\phi', \quad p = \left(\frac{a^2 g\rho}{h_0}\right)p',$$

and then, for convenience, the primes are dropped; here g is the gravitational acceleration, ρ is the water density, $c_0 = (gh_0)^{\frac{1}{2}}$ is the linear long-wave speed on water of uniform depth h_0, l is a typical wavelength and a is a typical wave amplitude. Note that, apart from the Froude number $F = U/c_0$, the long-wave parameter $\mu = h_0/l$, and the nonlinearity parameter $\epsilon = a/h_0$, two additional independent dimensionless parameter arise:

$$\beta = \frac{h_0}{L}, \quad \sigma = \frac{h_0}{w};$$

β is a measure of the slope of the channel sidewalls, while σ measures the channel width relative to the water depth and, as will be seen shortly, also controls three-dimensional effects.

Attention is focused now on weakly nonlinear, long waves propagating along a wide channel; thus, the parameters ϵ, μ and σ are taken to be small ($\epsilon, \mu, \sigma \ll 1$). Moreover, as already indicated, it is assumed that the channel cross-section is such that depth variations are confined close to the sidewalls ($\sigma/\beta = L/w \ll 1$), which then suggests the use of matched asymptotic expansions.

2.1. *Outer expansion*

The main part of the channel, away from the sloping boundaries ($1/\beta \ll z \ll 2/\sigma - 1/\beta$) forms an outer region where the water depth is uniform. Katsis & Akylas (1987*a*) have already developed an asymptotic theory for long waves excited by a pressure distribution moving at transcritical speed on water of uniform depth; so the analysis in the outer region follows closely their analysis, and only the main results will be highlighted here.

At transcritical Froude number, $F = 1 + \lambda\mu^2$ ($\lambda = O(1)$), waves evolve on the 'slow' time $T = \mu^2 t$ owing to weak nonlinear, dispersive and three-dimensional effects, which are taken to be equally important. To include nonlinearity and dispersion at the same order, the choice $\epsilon = \mu^2$ is made; furthermore, a balance with three-dimensional effects is achieved by introducing the stretched (outer) spanwise variable $Z = \epsilon z$, so that waves propagate predominantly along the x-direction. Based on these scalings, three-dimensional effects are expected to become appreciable when the channel is sufficiently wide, such that the extent of the outer region, in terms of Z, is $O(1)$:

$$\sigma = O(\epsilon) \quad \text{or} \quad W = \epsilon \frac{w}{h_0} = O(1). \tag{1}$$

Now, in terms of the scaled coordinates, Laplace's equation for ϕ and the bottom boundary condition at $y = -1$ give

$$\phi(x, Z, T; y) = f(x, Z, T) - \frac{\epsilon}{2!}(y+1)^2 f_{xx} + \frac{\epsilon^2}{4!}(y+1)^4 f_{xxxx} - \frac{\epsilon^2}{2!}(y+1)^2 f_{ZZ} + \dots . \tag{2}$$

The free-surface boundary conditions at $y = \epsilon\eta$ then imply that f is related to η through

$$\eta = -f_x + \epsilon(-p + \tfrac{1}{2} f_{xxx} - f_T - \lambda f_x - \tfrac{1}{2} f_x^2) + O(\epsilon^2), \tag{3}$$

and η satisfies the forced KP equation:

$$\eta_{Tx} + \lambda\eta_{xx} - \tfrac{3}{4}(\eta^2)_{xx} - \tfrac{1}{6}\eta_{xxxx} - \tfrac{1}{2}\eta_{ZZ} = \tfrac{1}{2} p_{xx} \quad (0 < Z < 2W). \tag{4}$$

In order to complete the formulation in the outer region, one needs to supplement (4) with boundary conditions at $Z = 0, 2W$. The appropriate boundary conditions will be obtained by matching the flow near the sidewalls with the outer flow. In preparation for this matching, it follows from (2), (3) that the inner limit of the outer flow as $Z \to 0^+$ is

$$\phi \sim f(x, 0, T) + \epsilon(z f_Z - \tfrac{1}{2}(y+1)^2 f_{xx}) + O(\epsilon^2), \tag{5a}$$

$$\eta \sim -f_x(x, 0, T) + \epsilon(\tfrac{1}{2} f_{xxx} - z f_{xZ} - f_T - \lambda f_x - \tfrac{1}{2} f_x^2) + O(\epsilon^2); \tag{5b}$$

for simplicity, it has been assumed that $p(x, Z)$ is localized close to the channel centreline ($Z = W$), and, thus, makes no contribution to η in (5*b*).

2.2. *Inner expansion*

It turns out that the form of the inner expansion and the resulting boundary conditions depends on the magnitude of the slope parameter β. In particular, if $\beta = O(1)$, the extent of the inner region is $O(h_0)$, which is small compared with both the channel width $2w$ and the typical wavelength l. On the other hand, if $\beta = O(\epsilon^{\frac{1}{2}})$, the extent of the inner region is now comparable with l (but still small compared with $2w$); so, on physical grounds, one would expect that in the latter case, the outer flow will be affected more seriously by the details of the depth variation close to the wall, and this should show up in the corresponding boundary conditions. Here, we shall confine our attention to $\beta = O(1)$ which is appropriate for comparing with the experiments of Sandover & Taylor (1962); the case $\beta = O(\epsilon^{\frac{1}{2}})$ is discussed in the Appendix.

For $\beta = O(1)$, the appropriate inner spanwise variable is z in the region close to the sidewall as $Z \to 0^+$. The governing equation is Laplace's equation

$$\epsilon\phi_{xx} + \phi_{yy} + \phi_{zz} = 0 \quad (-h(z) < y < 0, z > 0), \tag{6}$$

subject to the free-surface boundary conditions, correct to $O(\epsilon)$,

$$\phi_y = \epsilon(\eta_x + \phi_z\eta_z - \phi_{yy}\eta) \quad (y = 0), \tag{7a}$$

$$\phi_x + \eta + \tfrac{1}{2}(\phi_y^2 + \phi_z^2) = -\epsilon(\phi_T + \lambda\phi_x + \tfrac{1}{2}\phi_x^2 + \tfrac{1}{2}\eta(\phi_y^2 + \phi_z^2)_y + \eta\phi_{xy}) \quad (y = 0), \tag{7b}$$

the bottom boundary condition

$$\phi_y + h_z\phi_z = 0 \quad (y = -h(z)), \tag{8}$$

and the matching conditions (5a, b) as $z \to \infty$.

Expanding ϕ and η in powers of ϵ,

$$\phi = \phi_0 + \epsilon\phi_1 + \epsilon^2\phi_2 + \ldots, \quad \eta = \eta_0 + \epsilon\eta_1 + \epsilon^2\eta_2 + \ldots,$$

and substituting into (6)–(8), a hierarchy of linear problems is obtained. To $O(1)$, taking into account (5a, b), it is readily found that $\phi_0 = f(x, 0, T)$, $\eta_0 = -f_x(x, 0, T)$. Proceeding to $O(\epsilon)$, we write

$$\phi_1 = zf_Z - \tfrac{1}{2}(y+1)^2 f_{xx} + u \quad (Z = 0), \tag{9}$$

so that u satisfies

$$u_{yy} + u_{zz} = 0 \quad (-h(z) < y < 0, z > 0), \tag{10}$$

$$u_y = 0 \quad (y = 0), \tag{11a}$$

$$u_y = (1-h)f_{xx} - h_z f_Z \quad (y = -h(z)), \tag{11b}$$

and, in view of (9), the matching condition (5a) becomes

$$u \to 0 \quad (z \to \infty). \tag{12}$$

The boundary-value problem for u, consisting of Laplace's equation (10) subject to the Neumann conditions (11) and the matching condition (12), has a solution if the compatibility condition

$$f_{xx}\int_0^\infty (1-h)\,\mathrm{d}z - f_Z\int_0^\infty h_z\,\mathrm{d}z = 0 \quad (Z = 0),$$

which follows from Green's theorem, is satisfied; or, in terms of $\eta = -f_x + O(\epsilon)$,

$$\eta_Z = \mathscr{A}\eta_{xx} \quad (Z = 0), \tag{13}$$

where

$$\mathscr{A} = \int_0^\infty (1-h)\,\mathrm{d}z$$

is the area under the depth profile in dimensionless variables. Condition (13) ensures that matching between the inner and outer flow is possible. Now the formulation of the outer flow is complete; it consists of the forced KP equation (4) subject to the boundary condition (13) at the two sidewalls, $Z = 0, 2W$. Note that the outer flow is insensitive to the exact geometry of the sidewalls; of course, if the sidewalls are vertical, $\mathscr{A} = 0$ and the familiar no-flux boundary condition used by Katsis & Akylas (1987*a*), is recovered.

It is worth noting that the propagation of long waves along a sloping beach (with $\beta = O(1)$) can be discussed as a special case of the present formulation; the KP equation (4) applies in $Z > 0$ and the boundary condition (13) holds at $Z = 0$. In particular, linear sinusoidal wave modes (in the absence of forcing, $p = 0$, $\lambda = 0$),

$$\eta = H(Z)\exp[\mathrm{i}(kx+\omega T)],$$

satisfy

$$H_{ZZ}+\nu^2 H = 0 \quad (Z > 0),$$

where $\nu^2 = 2k(\omega+\frac{1}{6}k^3)$, subject to the boundary conditions

$$H_Z = -k^2\mathscr{A}H \quad (Z = 0)$$

and H bounded as $Z\to\infty$. This boundary-value problem for H has two kinds of solutions: for

$$\omega = -\tfrac{1}{2}k^3(\tfrac{1}{3}+\mathscr{A}^2), \tag{14}$$

there is an edge-wave mode ($H\to 0$ as $Z\to\infty$),

$$H = \exp(-k^2\mathscr{A}Z);$$

in addition, for $\omega > -\frac{1}{6}k^3$ there is a continuous spectrum representing the obliquely incident and reflected waves at the beach:

$$H = \sin\nu Z - \frac{\nu}{k^2\mathscr{A}}\cos\nu Z.$$

We remark that the dispersion relation (14) is in agreement with the earlier work of Grimshaw (1974), who studied linear long edge waves in an ocean of finite depth.

3. Undular bore

Suppose that, in an infinitely long, uniform channel, there is a gate that separates water at two different levels on either side. If the gate is suddenly removed, water advances into the region of lower depth forming a bore. It has been observed experimentally that, when the ratio of initial water depths exceeds a threshold value (of about 1.28), the resulting bore is short and turbulent, while below this threshold, it is laminar and consists of undulations (see, for example, Lighthill 1978, §2.12). In the latter case, one can use long-wave theory to describe the development of a bore because the undulations are long compared with the water depth. In a channel with rectangular cross-section, where the waves are straight crested, KdV theory predicts that an undular bore ultimately develops into a train of cnoidal waves of slowly varying amplitude and period, the leading wave being a solitary wave (Peregrine 1966; Fornberg & Whitham 1978). Three-dimensional bores were studied in the laboratory by Sandover & Taylor (1962) in channels with trapezoidal cross-sections.

Here, data from their experiments are used to make some comparisons with theoretical predictions based on the asymptotic theory presented earlier.

The formulation of the bore problem follows as a special case of the discussion in §2. As there is no forcing, we set $p = \lambda = 0$ in (4); furthermore, assuming that the channel is symmetric, it suffices to consider half the channel, $0 < Z < W$, and in addition to the boundary condition (13) at $Z = 0$, impose a symmetry condition at $Z = W$:

$$\eta_{Tx} - \tfrac{3}{4}(\eta^2)_{xx} - \tfrac{1}{6}\eta_{xxxx} - \tfrac{1}{2}\eta_{ZZ} = 0 \quad (-\infty < x < \infty, 0 < Z < W), \tag{15}$$

$$\eta_Z = \mathscr{A}\eta_{xx} \quad (Z = 0), \tag{16a}$$

$$\eta_Z = 0 \quad (Z = W). \tag{16b}$$

The appropriate initial conditions are

$$\eta(x, Z, T = 0) = 0 \quad (x < 0), \quad \eta(x, Z, T = 0) = \eta_\infty \quad (x \geqslant 0), \tag{17a}$$

while far upstream and downstream the conditions

$$\eta \to 0 \quad (x \to -\infty, T > 0), \quad \eta \to \eta_\infty \quad (x \to \infty, \quad T > 0) \tag{17b}$$

apply, where η_∞ is the initial difference in water levels.

The KP equation was solved numerically using the explicit, conditionally stable finite-difference scheme of Katsis & Akylas (1987*a*) with grid size $\Delta x = 0.07$, $\Delta Z = 0.021$ and time step $\Delta T = 0.5 \times 10^{-4}$. The boundary conditions (16) were approximated by centred differences in the x- and one-sided differences in the Z-directions. The upstream and downstream conditions (17*b*) were applied at the end points of the computational domain. Special care was taken that the finite extent of the computational domain did not affect the results reported here. In particular, from (15) and (16) together with mass conservation, it follows that

$$\int_{-\infty}^{\infty} [\eta(x, Z, T) - \eta(x, Z, T = 0)]\,\mathrm{d}x = 0; \tag{18}$$

is these calculations, the above constraint was satisfied to within 3%.

Sandover & Taylor (1962) conducted their experiments in channels with trapezoidal cross-sections, keeping the width at the bed constant at 12 in. while the sidewalls were supported at various angles θ to the vertical; also the still-water depth was kept constant at 3 in. Thus, in terms of θ, the parameter $\mathscr{A}$ is given by

$$\mathscr{A} = \tfrac{1}{2}\tan\theta. \tag{19}$$

Wave-height measurements were taken for a range of different discharges, using gauges which were located at several points across the channel at a distance 48 ft. from the inlet. The initial discharge Q, as measured in the laboratory, made dimensionless with $c_0 h_0^2$, is related to the theoretical parameters η_∞, $\mathscr{A}$, W and ϵ through

$$Q = 2W(\eta_\infty + \tfrac{3}{4}\epsilon\eta_\infty^2) - \epsilon\eta_\infty\mathscr{A}. \tag{20}$$

The parameter ϵ is specified by normalizing the dimensionless channel width at the free surface, $2W$, to be equal to unity; from (1) and the cross-section geometry, one then has

$$\epsilon = \frac{1}{2(2 + \tan\theta)}. \tag{21}$$

Numerical computations were carried out for two sidewall inclinations $\theta = \frac{1}{4}\pi, \frac{1}{3}\pi$. Using (19), (21), it is found that the corresponding values of $\mathscr{A}$ are 0.5, 0.866 and those of ϵ are 0.167 and 0.134. Figures 2(*a*) and 2(*b*), respectively, show perspective

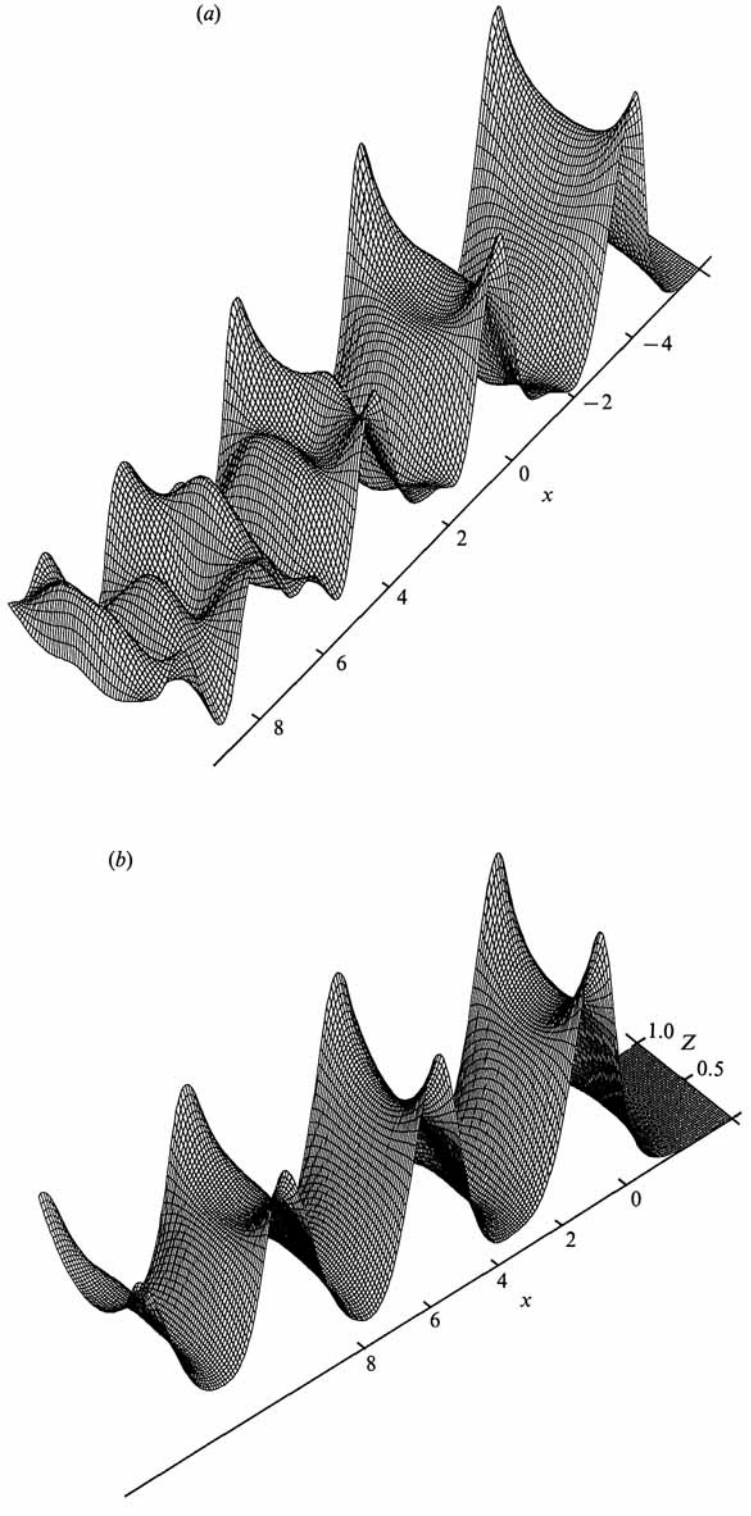

FIGURE 2. Computed free surface at the head of undular bores in sloped-wall channels. (a) Sidewall slope $\theta = \frac{1}{4}\pi$, water-level difference $\eta_\infty = 1.08$, time $T = 12.5$; (b) $\theta = \frac{1}{3}\pi$, $\eta_\infty = 1.13$. $T = 9.5$.

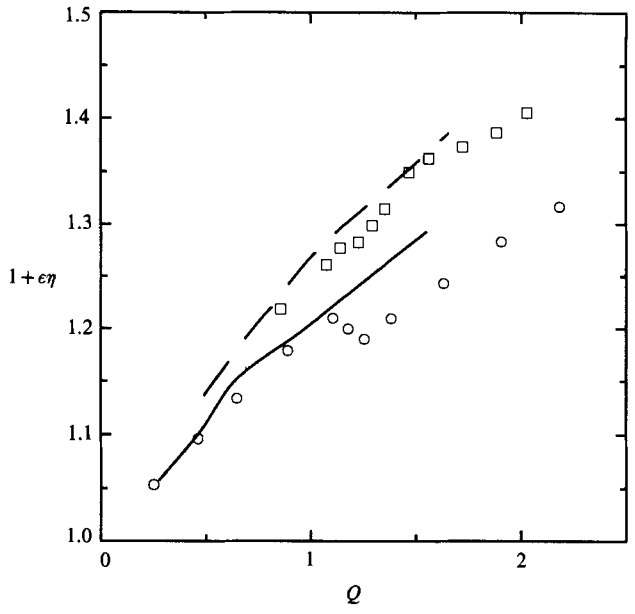

FIGURE 3. Comparison of the theoretical predictions of wave height of the leading crest (at the channel centreline) of undular bores, with the laboratory measurements of Sandover & Taylor (1962) for two sidewall inclinations θ: ——, theory, $\theta = \frac{1}{4}\pi$; □, experiment, $\theta = \frac{1}{4}\pi$; ——, theory, $\theta = \frac{1}{3}\pi$; ○, experiment, $\theta = \frac{1}{3}\pi$.

views of the computed free surface for $\theta = \frac{1}{4}\pi$ with $\eta_\infty = 1.08$, and for $\theta = \frac{1}{3}\pi$ with $\eta_\infty = 1.13$, which correspond to the same value of $Q = 1.13$ (this gives a discharge of 90 gals/min), according to (20). In both cases, these snapshots are taken as the leading crest of the bore crosses the streamwise position at which the gauges were placed in the experiment; the corresponding times turn out to be $T = 12.5, 9.5$, respectively. The three-dimensional structure of the bore is quite evident, and there is, at least qualitatively, a resemblance to the photographs from the experiments of Sandover & Taylor (1962): wave crests are curved across the channel and steeper close to the sidewalls, where wave breaking is more likely to occur; some of the individual wave undulations tend to form a double-hump structure, having two crests separated by a shallow trough in the middle. Also it is interesting to note that changing $\mathscr{A}$ from 0.5 to 0.866 causes the wave pattern to become more uniform; this feature will be discussed more thoroughly later (see §5), in connection with waves of permanent form.

Turning now to a quantitative comparison of theory with experiment, figure 3 shows a plot of the leading-wave-crest height at the channel centreline as a function of Q. For both values of θ, the theoretical predictions are in good agreement with experiment, until Q is large enough for wave breaking to occur in the experiment, which is, of course, not taken into account in the theory; wave breaking was first observed at $Q \approx 1.5$ for $\theta = \frac{1}{4}\pi$ and at $Q \approx 1.15$ for $\theta = \frac{1}{3}\pi$, as is evident from the sudden dip of the experimental data points in figure 3, near those values of Q. Figures 4(*a*) and 4(*b*) show comparisons of the theoretical with the experimental profiles of the leading wave crest along the channel centreline, for $\theta = \frac{1}{4}\pi, \frac{1}{3}\pi$, respectively, and at the same $Q = 1.13$. Again, the agreement between theory and experiment is very good; in fact, this provides a rather severe test of the theory because, as is clear from

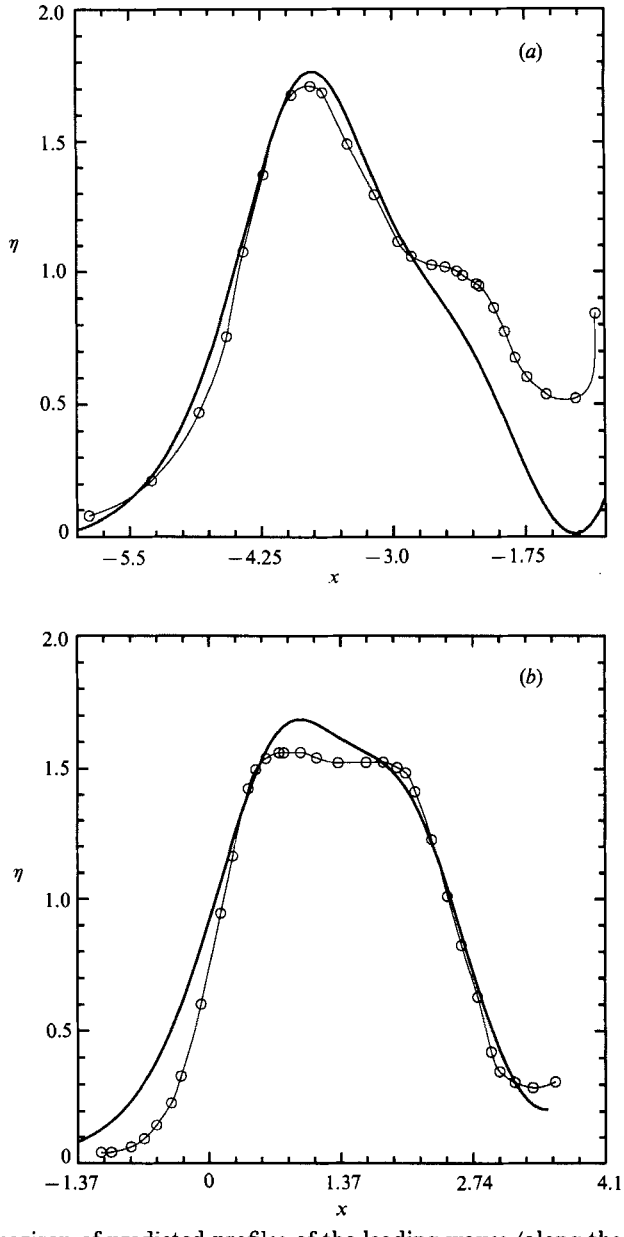

FIGURE 4. Comparison of predicted profiles of the leading waves (along the centreline) of undular bores with those measured by Sandover & Taylor (1962): ——, theory; —⊖—, experiment. (*a*) $\theta = \frac{1}{4}\pi$, $T = 12.5$; (*b*) $\theta = \frac{1}{3}\pi$, $T = 9.5$.

experimental observations, changing θ from $\frac{1}{4}\pi$ to $\frac{1}{3}\pi$ alters the wave profile quite significantly. In addition, it should be kept in mind that, in the experiments of Sandover & Taylor (1962), the channel geometry does not suggest a very thin boundary region with a wide core region, as postulated in the model – the values of ϵ are only moderately small. On the other hand, the good agreement between theory and experiment indicates that the channel is wide enough for three-dimensional effects to be important.

4. Upstream response due to transcritical forcing

We now turn our attention to the wave pattern generated by a pressure distribution moving at transcritical speed ($F \approx 1$). As already indicated, for a channel with vertical sidewalls, it is now known (see Wu 1987; Akylas 1988 and references given there) that, regardless of the shape of the forcing, there is a strong upstream response which consists of a uniform train of straight-crested KdV solitary waves; of course, it is the presence of vertical sidewalls that allows these particular waves to form, and in the context of the present model, it is of interest to examine the extent to which the upstream disturbance is affected by sloping sidewalls.

The pressure distribution is assumed to move along the channel centreline and is taken to have a Gaussian form along x and to be localized in the spanwise direction:

$$p(x, Z) = \pi^{\frac{1}{2}} p_0 \exp(-x^2)\, \delta(Z-W), \tag{22}$$

where p_0 is a constant and δ is the Dirac delta function. Assuming, furthermore, that the channel is symmetric and the forcing is turned on impulsively, (4), (13), (22) then lead to the following initial-boundary-value problem:

$$\eta_{Tx} + \lambda \eta_{xx} - \tfrac{3}{4}(\eta^2)_{xx} - \tfrac{1}{6}\eta_{xxxx} - \tfrac{1}{2}\eta_{ZZ} = 0 \quad (-\infty < x < \infty, 0 < Z < W), \tag{23}$$

$$\eta_Z = \mathscr{A}\eta_{xx} \quad (Z = 0), \tag{24a}$$

$$\eta_Z = \tfrac{1}{2}\pi^{\frac{1}{2}} p_0 (\exp(-x^2))_{xx} \quad (Z = W), \tag{24b}$$

$$\eta = 0 \quad (T = 0). \tag{25}$$

The above problem is solved numerically using the method of Katsis & Akylas (1987*a*) with the same resolution as in the bore problem discussed in §3, and by normalizing the channel width $2W$ to unity. Again, the constraint (18), which ensures mass conservation, was satisfied to within a few percent.

Numerical computations indicate that the nature of the upstream response depends crucially on the value of $\mathscr{A}$. For small $\mathscr{A}$ (≈ 0.1), the individual upstream waves remain straight while wave crests climb and troughs dip near the sidewalls, as expected from the wall condition (24*a*). On increasing $\mathscr{A}$ further, the upstream wave disturbance loses its periodic appearance entirely and becomes highly disordered. Figure 5(*a*) shows the response for $\mathscr{A} = 0.5$ ($p_0 = 10$, $\lambda = -0.5$) at $T = 4$. Note that the individual waves are quite different from each other and there are large spanwise variations. However, for values of $\mathscr{A}$ around 1, the upstream wavetrain is still fully three-dimensional but, quite remarkably, it regains its uniform structure, as indicated in figure 5(*b*) for $\mathscr{A} = 1$ ($p_0 = 10$, $\lambda = -1$) at $T = 4$; each of the upstream waves now has sharp crests at the walls that split into two humps towards the centreline, and the troughs are nearly flat and broad. We remark that a similar tendency for the wave pattern to become more regular was also observed in the development of a bore, when $\mathscr{A}$ was changed from 0.5 to 0.866.

5. Waves of permanent form

As remarked earlier, in a channel with vertical sidewalls, there is a close relation between the development of an undular bore and periodic waves of permanent form (cnoidal waves), which, in fact, can be used to construct approximate solutions based on modulation theory (Gurevich & Pitaevskii 1974; Fornberg & Whitham 1978); this also turns out to be the case for the upstream response due to near-resonant forcing,

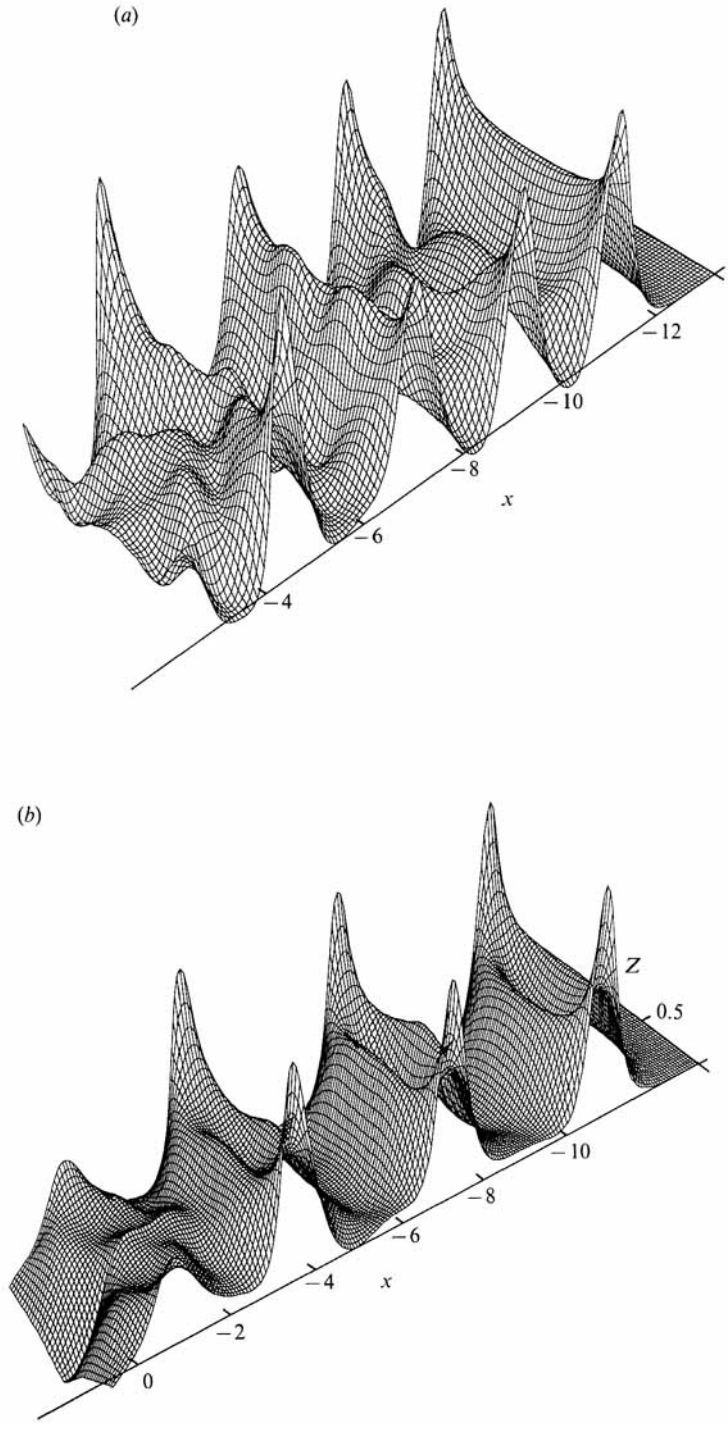

FIGURE 5. Upstream waves excited by transcritical forcing in sloped-wall channels, at $T = 4$ and $p_0 = 10$: (a) $\mathscr{A} = 0.5$, $\lambda = -0.5$; (b) $\mathscr{A} = 1.0$, $\lambda = -1.0$.

as pointed out recently by Smyth (1987). Accordingly, in order to gain some insight into these wave phenomena in the presence of sloping sidewalls – in particular the crucial dependence on $\mathscr{A}$ noted in §§3, 4 – here we look for periodic waves of permanent form. To this end, η is assumed to depend on $\xi = x + cT$, c being the phase speed, and on using (4) (with $p = 0$, $\lambda = 0$), (13) and taking the channel to be symmetric, one has

$$-c\eta_{\xi\xi} + \tfrac{3}{4}(\eta^2)_{\xi\xi} + \tfrac{1}{6}\eta_{\xi\xi\xi\xi} + \tfrac{1}{2}\eta_{ZZ} = 0 \quad (-\xi_0 < \xi < \xi_0, 0 < Z < W), \tag{26}$$

$$\eta_Z = \mathscr{A}\eta_{\xi\xi} \quad (Z = 0), \tag{27a}$$

$$\eta_Z = 0 \quad (Z = W), \tag{27b}$$

where $2\xi_0$ is the period; furthermore, the water depth is fixed by setting $\eta(\xi = \xi_0, Z = 0) = 0$. When $\mathscr{A} = 0$, cnoidal waves with no Z-variations are solutions of the above system, and the KdV solitary wave is obtained as a limiting case as the period is increased. Our goal here is to examine the effect of $\mathscr{A}$ on these known wave solutions.

5.1. *Numerical results*

Equations (26) and (27) are solved numerically using a combination of spectral and finite-difference methods. Assuming that waves are symmetric about $\xi = 0$, Fourier, spectral differentiation is used to calculate derivatives with respect to ξ, while derivatives with respect to Z are approximated by second-order finite differences. Thus for given values of the speed c, slope parameter $\mathscr{A}$, and half-period ξ_0, equation (26) and the boundary conditions (27) yield a nonlinear algebraic system for the unknown values of η at the grid points, which is solved through Newton's method. As a check, these numerical solutions were verified against results obtained independently from a second technique, using a shooting procedure. The basis for discretization is the same as in the first method – Fourier expansion in ξ and second-order, finite differences in Z; but the desired solution is found by starting with guessed values for η at the centreline $Z = W$, where (27*b*) is applied, and then marching along lines of constant ξ towards the sloping wall at $Z = 0$. The assumed values of η at $Z = W$ are systematically corrected through Newton iteration and the marching procedure is repeated until the wall condition (27*a*) is also met. Furthermore, for periodic waves, the constraint analogous to (18) is that

$$\int_{-\xi_0}^{\xi_0} \eta(\xi, Z)\, \mathrm{d}\xi$$

is independent of Z; the numerical solutions were checked against this constraint.

Starting with the known cnoidal-wave solution at $\mathscr{A} = 0$, continuation in $\mathscr{A}$ was used to compute solution families for $\mathscr{A} > 0$ and for a range of phase speeds, $0.5 \leqslant c \leqslant 2.5$ (the upstream waves shown in figure 5(*b*) travel with a speed of, approximately, 2.5). The channel width $2W$ is normalized to unity in all cases discussed below, though the waves seem to be relatively insensitive to changes in W. The period $2\xi_0$ is taken to be 2π; cnoidal waves having this period and $0.5 \leqslant c \leqslant 2.5$ appear essentially as a series of KdV solitary waves, with very little interaction between individual crests. Numerical computations indicate that, as the speed c is increased for fixed $\mathscr{A}$, the wave structure remains qualitatively the same but, as one would expect, wave crests become steeper and three-dimensional features such as crest curvature, both in plan and elevation, become more pronounced. On the other hand, varying $\mathscr{A}$ gives rise to more dramatic effects: for small values of $\mathscr{A} > 0$, there

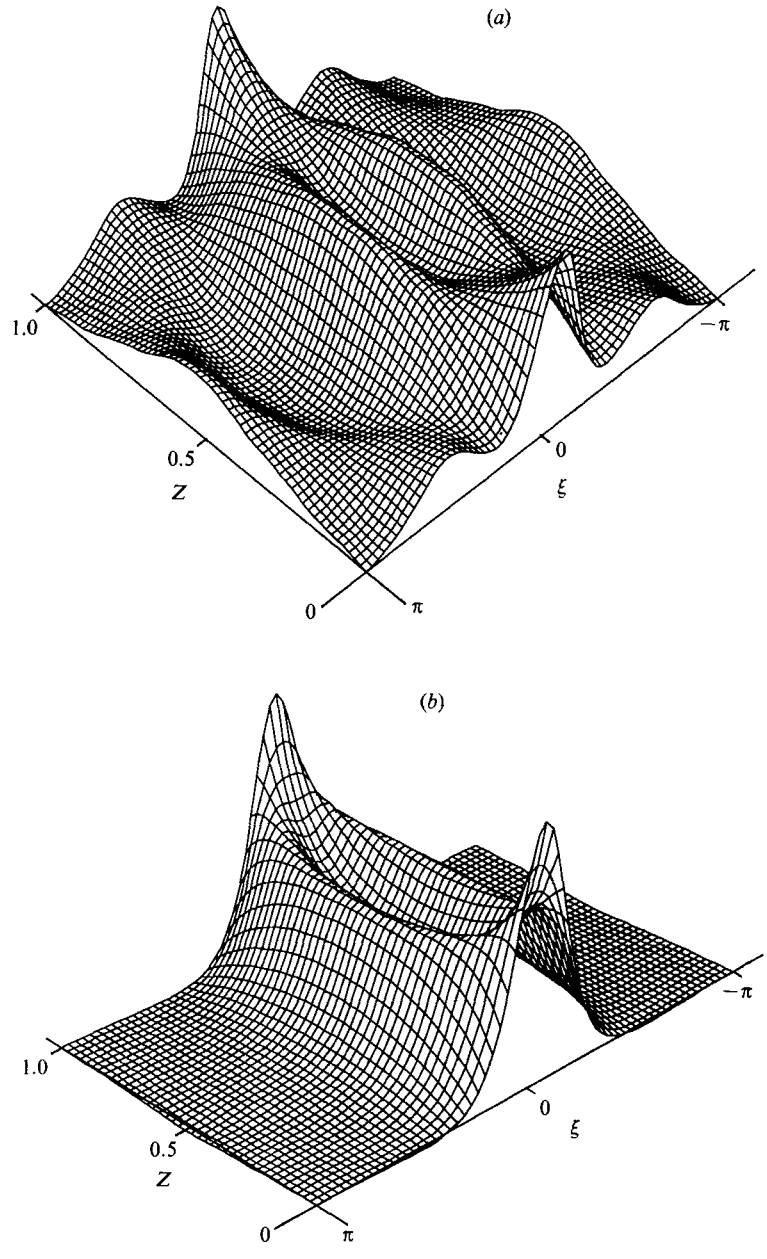

FIGURE 6. Periodic waves of permanent form of period $2\xi_0 = 2\pi$, speed $c = 2.5$ and channel width $2W = 1$. (*a*) $\mathscr{A} = 0.5$. (*b*) $\mathscr{A} = 1.0$.

appear small oscillatory tails and the crest acquires a depression near the centreline. Figure 6(*a*) shows a perspective view of the free surface corresponding to $c = 2.5$ and $\mathscr{A} = 0.5$, at which point these effects have become quite strong and the wave has a fairly complicated three-dimensional structure. With further increase in $\mathscr{A}$, however, the oscillations at the tails tend to subside resulting in broad, nearly flat troughs for values of $\mathscr{A}$ around 1, as shown in figure 6(*b*). These computations were carried out using a resolution of 33 grid points in $0 \leqslant \xi \leqslant \pi$; in the spanwise direction,

$0 \leqslant Z \leqslant 0.5$, 31 grid points were used in the first case, and 21 points in the second case.

Based on the above numerical calculations of steady waves, it is now possible to explain certain features of the unsteady wave patterns noted earlier. In particular, there is a striking similarity between the waves with the double-hump structure found in the upstream response for $\mathscr{A} = 1$ (see figure 5*b*), and the steady waves shown in figure 6(*b*) for the same value of $\mathscr{A}$. Figure 6(*b*) also suggests that there is little interaction between waves in neighbouring periods, so that each of these waves is expected to propagate more or less as a separate entity; the upstream response shown in figure 5(*b*), which consists of a series of these waves, seems to support this claim. On the other hand, the relatively non-uniform appearance of the upstream response for $\mathscr{A} = 0.5$ (see figure 5*a*) is probably due to the large spanwise variations at the tails of the steady waves shown in figure 6(*a*), which cause individual waves to interact in a complicated way. The same reasoning also seems to provide an explanation for the more uniform appearance of the undular bore for $\mathscr{A} = 0.866$ as compared to that for $\mathscr{A} = 0.5$ (figure 2*a*, *b*).

A question that has not been addressed so far, is whether solitary waves exist for $\mathscr{A} > 0$. Assuming that solitary waves can be obtained from periodic waves in the limit that the wave period becomes large, one could use continuation in ξ_0 to search for possible solitary waves numerically; this is a computationally expensive task and will not be pursued here. Another approach is to use perturbation theory for $\mathscr{A} \ll 1$, as discussed below.

5.2. *Perturbation theory for* $\mathscr{A} \ll 1$

Assuming that $\mathscr{A} \ll 1$, η is expanded in powers of $\mathscr{A}$:

$$\eta(\xi, Z) = \eta^{(0)}(\xi) + \mathscr{A}\eta^{(1)}(\xi, Z) + \mathscr{A}^2\eta^{(2)}(\xi, Z) + \ldots, \tag{28}$$

where $\eta^{(0)}$ is the KdV solitary wave,

$$\eta^{(0)} = a_0 \operatorname{sech}^2 \alpha\xi \tag{29a}$$

with

$$\alpha = (\tfrac{3}{4}a_0)^{\frac{1}{2}}, \quad c = \tfrac{1}{2}\alpha. \tag{29b}$$

Upon substitution of (28), (29) into (26), (27), it is found that $\eta^{(1)}$ satisfies a linear inhomogeneous problem. It proves convenient to write

$$\eta^{(1)} = \frac{2W}{\pi}\eta^{(0)}_{\xi\xi} \sin\frac{\pi Z}{2W} + \tilde{\eta}(\xi, Z),$$

so that $\tilde{\eta}$ satisfies a problem with homogeneous boundary conditions:

$$(-c\tilde{\eta} + \tfrac{3}{2}\eta^{(0)}\tilde{\eta} + \tfrac{1}{6}\tilde{\eta})_{\xi\xi} + \tfrac{1}{2}\tilde{\eta}_{ZZ} = \mathscr{R}, \tag{30}$$

$$\tilde{\eta}_Z = 0 \quad (Z = 0, W), \tag{31}$$

where

$$\mathscr{R} = \left\{c\eta^{(0)} + \frac{W}{\pi}\sin\frac{\pi Z}{2W}\left[3(\eta^{(0)}_\xi)^2 + \left(\frac{\pi}{2W}\right)^2 \eta^{(0)}\right]\right\}_{\xi\xi}.$$

The solution of (30), (31) is posed as a Fourier series

$$\tilde{\eta} = \sum_{n=0}^{\infty} G^{(n)}(\xi) \cos\frac{n\pi Z}{W}$$

which meets the boundary conditions (31) automatically. The Fourier coefficients are to be determined by solving a sequence of ordinary differential equations:

$$[-cG^{(n)}+\tfrac{3}{2}\eta^{(0)}G^{(n)}+\tfrac{1}{6}G^{(n)}_{\xi\xi}]_{\xi\xi}-\frac{1}{2}\left(\frac{n\pi}{W}\right)^2 G^{(n)}=\mathscr{R}^{(n)} \quad (n=0,1,2,\ldots), \tag{32}$$

where
$$\mathscr{R}^{(0)}=\left[\frac{6W}{\pi^2}(\eta^{(0)}_{\xi})^2+\frac{1}{2W}\eta^{(0)}\right]_{\xi\xi},$$

and
$$\mathscr{R}^{(n)}=\frac{4W}{\pi^2(1-4n^2)}\left[3(\eta^{(0)}_{\xi})^2+\left(\frac{\pi}{2W}\right)^2\eta^{(0)}\right]_{\xi\xi} \quad (n=1,2,3,\ldots).$$

Furthermore, for η to remain localized in the x-direction, we require

$$G^{(n)}(\xi)\to 0 \quad (\xi\to\pm\infty) \tag{33}$$

for all n.

Now the solution of (32) subject to (33) can be readily found for $n=0$:

$$G^{(0)}=\frac{6W}{\pi^2}a_0^2(3S^4-2S^2)+\frac{1}{W}(S^2-\alpha\xi RS^2), \tag{34}$$

where $S\equiv\operatorname{sech}\alpha\xi$, $R\equiv\tanh\alpha\xi$. The last term in (34) is secular and makes the expansion (28) non-uniform as $\xi\to\pm\infty$; however, noting that

$$\frac{\partial}{\partial a_0}(a_0S^2)=S^2-\alpha\xi RS^2,$$

this non-uniformity can be interpreted as a slight change in the amplitude, a_0, of the KdV solitary wave (29). On the other hand, we argue that, in general, one cannot find a solution of (32) that satisfies (33) for $n\geqslant 1$: as $|\xi|\to\infty$, the four homogeneous solutions of (32) behave like

$$\exp(\pm q\xi), \quad \exp(\pm ir\xi), \tag{35}$$

where
$$q^2=3c+\left[9c^2+3\left(\frac{n\pi}{W}\right)^2\right]^{\frac{1}{2}}, \quad r^2=-3c+\left[9c^2+3\left(\frac{n\pi}{W}\right)^2\right]^{\frac{1}{2}},$$

and only one of these solutions is consistent with (33). Accordingly, in order to find a smooth solution of the inhomogeneous equation (32), one needs to include a contribution from the homogeneous solutions (35) with oscillating behaviour as well, thus violating (33). Therefore, it is concluded that no solitary waves are possible for $\mathscr{A}\ll 1$; this seems to be consistent with our numerical calculations which indicate that small-amplitude oscillations, owing to cross-modes corresponding to $n\geqslant 1$ in (32), appear at the tails when $\mathscr{A}$ is small. It is interesting to note that, in this respect, there is an analogy with long-wave propagation in a slowly rotating channel: solitary waves do not seem to exist in this case either, owing to the radiation of Poincaré waves which are the corresponding cross-modes (Katsis & Akylas 1987*b*; Melville, Thomasson & Renouard 1989). Of course, as the perturbation theory is expected to be valid only for $\mathscr{A}\ll 1$, it is still possible that solitary waves may exist for other parameter values; for example, figure 6(*b*) suggests that perhaps such waves could be found for values of $\mathscr{A}$ around 1.

This work was supported by the Office of Naval Research under project NR062-742 and by the National Science Foundation Grant MSM-8451154.

Appendix. Wall boundary condition for $\beta = O(\epsilon^{\frac{1}{2}})$

When $\beta = O(\epsilon^{\frac{1}{2}})$, the analysis presented in §2.2 needs to be modified. Here we sketch the main steps in the inner expansion, which lead to the wall boundary condition, appropriate in this case.

Focusing attention on the inner region $Z \to 0^+$, the rigid bottom is at $y = -h(\tilde{z})$, where $\tilde{z} = \epsilon^{\frac{1}{2}} z$ is the inner spanwise coordinate. In terms of the inner variables, the governing equations, correct to $O(\epsilon)$, are

$$\epsilon(\phi_{xx} + \phi_{\tilde{z}\tilde{z}}) + \phi_{yy} = 0 \quad (-h < y < 0, \tilde{z} > 0), \tag{A 1}$$

$$\phi_y = \epsilon(\eta_x - \phi_{yy}\eta) \quad (y = 0), \tag{A 2a}$$

$$\phi_x + \eta + \tfrac{1}{2}\phi_y^2 = -\epsilon(\phi_T + \lambda\phi_x + \tfrac{1}{2}\phi_x^2 + \eta\phi_y\phi_{yy} + \eta\phi_{xy}) \quad (y = 0), \tag{A 2b}$$

$$\phi_y = -\epsilon h_{\tilde{z}}\phi_{\tilde{z}} \quad (y = -h(\tilde{z})), \tag{A 3}$$

together with the matching conditions (5a, b) as $\tilde{z} \to \infty$. To solve this problem we write

$$\phi = \chi(x, \tilde{z}, T) - \epsilon v(x, y, \tilde{z}, T) + \ldots,$$

and upon substitution into (A 1)–(A 3), it is found that v satisfies

$$v_{yy} = \chi_{xx} + \chi_{\tilde{z}\tilde{z}} \quad (-h < y < 0, \tilde{z} > 0), \tag{A 4}$$

$$v_y = \chi_{xx} \quad (y = 0), \tag{A 5}$$

$$v_y = h_{\tilde{z}}\chi_{\tilde{z}} \quad (y = -h(\tilde{z})). \tag{A 6}$$

In addition, the matching condition (5a) implies

$$\chi \sim f + \epsilon^{\frac{1}{2}}\tilde{z} f_Z \quad (Z = 0, \tilde{z} \to \infty), \tag{A 7a}$$

$$v \sim \tfrac{1}{2}(y+1)^2 f_{xx} - \tfrac{1}{2}\tilde{z}^2 f_{ZZ} \quad (Z = 0, \tilde{z} \to \infty). \tag{A 7b}$$

The solution of (A 4)–(A 6), consistent with (A 7b), is

$$v = \tfrac{1}{2}(y+1)^2\chi_{xx} + \tfrac{1}{2}y^2\chi_{\tilde{z}\tilde{z}} - \tfrac{1}{2}\tilde{z}^2 f_{ZZ},$$

subject to the compatibility condition

$$(h\chi_{\tilde{z}})_{\tilde{z}} + (h-1)\chi_{xx} = 0 \quad (\tilde{z} > 0). \tag{A 8}$$

Note that $h = 0$ at the shoreline $\tilde{z} = 0$, so that in general, solutions of (A 8) are expected to be singular there; requiring that χ is regular at $\tilde{z} = 0$ and imposing the matching condition (A 7a) determine the desired boundary condition at $Z = 0$ for the outer flow. The details depend on the specific depth profile $h(\tilde{z})$; here we work out the particular case of exponential depth variation,

$$h(\tilde{z}) = 1 - \mathrm{e}^{-\tilde{z}}. \tag{A 9}$$

Taking Fourier transforms in x, the solution of (A 8) is

$$\chi = \int_{-\infty}^{\infty} \hat{\chi}(k; \tilde{z}, T)\,\mathrm{e}^{\mathrm{i}kx}\,\mathrm{d}k,$$

where $\hat{\chi}$ satisfies

$$(h\hat{\chi}_{\tilde{z}})_{\tilde{z}} + k^2(h-1)\hat{\chi} = 0 \quad (\tilde{z} > 0). \tag{A 10}$$

Now, for the exponential depth profile (A 9), the solution of (A 10) that is regular at $\tilde{z} = 0$ can be related to hypergeometric functions (Ball 1967), and its asymptotic behaviour as $\tilde{z} \to \infty$ is found to be

$$\hat{\chi} \sim D(1 - K(k)\tilde{z}) \quad (\tilde{z} \to \infty), \tag{A 11}$$

where D is an as yet unspecified constant, and

$$K(k) = \frac{1}{2\gamma + \psi(a_+) + \psi(a_-)};$$

here ψ is the digamma function (Abramowitz & Stegun 1964, p. 258), γ is Euler's constant, and

$$a_\pm = \tfrac{1}{2} \pm \tfrac{1}{2}(1+4k^2)^{\frac{1}{2}}.$$

Comparing (A 11) with (A 7a), matching is achieved if

$$\epsilon^{\frac{1}{2}} \hat{f}_Z + K(k)\hat{f} = 0 \quad (Z = 0), \tag{A 12}$$

or, equivalently in terms of $\eta = -f_x + O(\epsilon)$, if

$$\epsilon^{\frac{1}{2}} \eta_Z + \int_{-\infty}^{\infty} K(k)\,\hat{\eta}\,\mathrm{e}^{\mathrm{i}kx}\,\mathrm{d}k = 0 \quad (Z = 0). \tag{A 13}$$

So, when $\beta = O(\epsilon^{\frac{1}{2}})$, the wall boundary condition takes the integral–differential form (A 13). Note that dropping the $O(\epsilon^{\frac{1}{2}})$-term in (A 12), (A 13) is inconsistent close to the zeros of $K(k)$ at

$$k = \pm(m(m+1))^{\frac{1}{2}} \quad (m = 1, 2, 3, \ldots);$$

these are the cut-off wavenumbers of edge-wave modes found by Ball (1967). Finally, we remark that the form of the boundary condition (A 13) remains valid for any depth variation $h(\tilde{z})$, but the function $K(k)$ depends on the particular depth profile.

REFERENCES

Abramowitz, M. & Stegun, I. A. 1964 *Handbook of Mathematical Functions.* Washington, D.C., National Bureau of Standards.

Akylas, T. R. 1988 Nonlinear forced wave phenomena. In *Nonlinear Wave Interactions in Fluids* (ed. R. W. Miksad, T. R. Akylas & T. Herbert), ASME AMD, Vol. 87, p. 157.

Ball, F. K. 1967 Edge waves in an ocean of finite depth. *Deep-Sea Res.* **14**, 79–88.

David, D., Levi, D. & Winternitz, P. 1989 Solitons in shallow seas of variable depth and in marine straits. *Stud. Appl. Maths* **80**, 1–23.

Fenton, J. D. 1973 Cnoidal waves and bores in uniform channels of arbitrary cross-section. *J. Fluid Mech.* **58**, 417–434.

Fornberg, B. & Whitham, G. B. 1978 A numerical and theoretical study of certain nonlinear wave phenomena. *Phil. Trans. R. Soc. Lond.* A **289**, 373–404.

Grimshaw, R. 1974 Edge waves: a long-wave theory for oceans of finite depth. *J. Fluid Mech.* **62**, 775–791.

Gurevich, A. V. & Pitaevskii, L. P. 1974 Nonstationary structure of a collisionless shock wave. *Sov. Phys.-JETP* **38**, 291–297.

Katsis, C. & Akylas, T. R. 1987*a* On the excitation of long nonlinear water waves by a moving pressure distribution. Part 2. Three-dimensional effects. *J. Fluid Mech.* **177**, 49–65.

Katsis, C. & Akylas, T. R. 1987*b* Solitary internal waves in a rotating channel: A numerical study. *Phys. Fluids* **30**, 297–301.

Kirby, J. T., Philip, R. & Vengayil, P. 1987 One-dimensional and weakly two-dimensional waves in varying channels: numerical examples. In *Nonlinear Water Waves* (ed. K. Horikawa & H. Maruo), pp. 357–364. Springer.

Lighthill, M. J. 1978 *Waves in Fluids.* Cambridge University Press.

Melville, W. K., Tomasson, G. G. & Renouard, D. P. 1989 On the stability of Kelvin waves. *J. Fluid Mech.* **206**, 1–23.

Peregrine, D. H. 1966 Calculations of the development of an undular bore. *J. Fluid Mech.* **25**, 321–330.

PEREGRINE, D. H. 1968 Long waves in a uniform channel of arbitrary cross-section. *J. Fluid Mech.* **32**, 353–365.

PEREGRINE, D. H. 1969 Solitary waves in trapezoidal channels. *J. Fluid Mech.* **35**, 1–6.

SANDOVER, J. A. & TAYLOR, C. 1962 Cnoidal waves and bores. *La Houille Blanche* **17**, 443–455.

SMYTH, N. F. 1986 Modulation theory solution for resonant flow over topography. *Proc. R. Soc. Lond.* A **409**, 79–97.

SUGIMOTO, N. & KAKUTANI, T. 1984 Reflection of a shallow-water soliton. Part 1. Edge layer for shallow-water waves. *J. Fluid Mech.* **146**, 369–382.

WHITHAM, G. B. 1974 *Linear and Nonlinear Waves.* Wiley-Interscience.

WU, T. Y. 1987 Generation of upstream advancing solitons by moving disturbances. *J. Fluid Mech.* **184**, 75–99.